Photomedicine and Laser Surgery
Volume 24, Number 3, 2006

Pp. 402–409

Feasibility of Three-Dimensional Optical Coherence Tomography and Optical Doppler Tomography of Malignancy in Hamster Cheek Pouches

NEVINE M. HANNA, M.P.H.,[1] WILLIAM WAITE, B.S.,[1] KATIE TAYLOR,[1] WOONG-GYU JUNG, M.S.,[1,2] DAVID MUKAI, B.S.,[1] ERIN MATHENY, B.S.,[1] KELLY KREUTER, B.A.,[1] PETRA WILDER-SMITH, D.D.S., Ph.D.,[1] MATTHEW BRENNER, M.D.,[1,3] and ZHONPING CHEN, Ph.D.[1,2]

ABSTRACT

Objective: **Hamster cheek pouches (HCP) with various degrees of 9,10-dimethyl-1,2-benzanthracene (DMBA)–induced dysplasia and malignancies were imaged with OCT/ODT *in vivo* and *in vitro* to assess the potential for three-dimensional high-resolution optical localization of airway malignancy.** ***Background Data:*** **Optical coherence tomography (OCT)/optical doppler tomography (ODT) provide potential capability for real-time *in vivo* high-resolution (2–20 μm) cross-sectional imaging of tissues and spatially resolved blood flow in microvasculature for pathology diagnostics.** ***Methods:*** **DMBA was applied to the right side of the cheek pouch (HCP), and mineral oil (control) to the left side three times weekly for 10–18 weeks in Syrian Golden Hamsters using a standard protocol for malignancy induction. HCP were imaged *in vivo* with OCT/ODT as well as *in vitro* post-excision, using a prototype 1310-nm broadband superluminescent diode-based OCT/ODT device constructed in our laboratory. Three-dimensional images were constructed, and compared to standard and three-dimensional histology hematoxylin and eosin staining.** ***Results and Conclusion:*** **OCT imaging offered exceptional resolution of the HCP to depths of 1–2 mm and confirmed ability to detect dysplasia and malignancy. Three-dimensional OCT images were readily constructed, allowing visualization of extent and localization of tumor margins. ODT demonstrated increased vascularity in the area of neoplasia. OCT/ODT is a promising new technology for oral airway diagnostics.**

INTRODUCTION

EARLY DETECTION OF CANCER and its curable precursors remains the best way to improve patient survival and quality of life in many fields, including oral cancers.[1–3] Optical coherence tomography (OCT) is a recently described, rapidly evolving imaging technology that enables high-resolution imaging of tissue. OCT has potential as a tool for improving the early diagnosis of dental and oral diseases, including oral cancer.[4] The first intraoral dental OCT images were reported in April 2000.[5] These images depicted both hard and soft oral tissues at high resolution and demonstrated the feasibility of OCT imaging in the oral cavity.

OCT technology has capabilities for outstanding resolution parameters (1–2 μm resolution has been reported), real-time visualization, and endoscopic access through rigid or flexible fiberoptic probe.[6–8] Current *in vivo* endoscopic OCT resolutions of 10–20 μm are substantially higher than available ultrasound probe resolutions, though depth of penetration is limited to about 2–3 mm.[6,9] OCT systems can be constructed at reasonable cost, can be modified for convenient application in the oral cavity, and may eventually allow clinicians to diagnose cancerous growths non-invasively, or help guide biopsy sites. Imaging can be performed with relatively inexpensive flexible fiberoptic imaging probes, enabling many clinically relevant tissue and organ surface, and subsurface structures to be imaged.[10,11]

[1]Irvine Beckman Laser Institute and [2]Department of Biomedical Engineering, University of California Irvine, Irvine, California.
[3]University of California Irvine Medical Center, Orange, California.

The principles of OCT are analogous to those of ultrasound. Conceptual comparisons between the two technologies have been made previously.[12–20] In OCT imaging, short-coherence-length broadband light reflectance is used, rather than sound, as the imaging source.[6] Because the reflectance delay times for light are extremely short, determination of the delays requires use of interferometry detection methods. For OCT, light is emitted from a broadband laser light source towards a partially reflecting mirror that acts as an optical beam splitter. One arm of the resulting light beams (the reference delay arm) is directed towards a precisely controlled mounting reference mirror at a specified distance from the beam splitter. The other beam (the sample arm) is aimed towards the biological tissue to be examined. Light directed toward the reference mirror reflects back with a specific time delay (proportional to the distance traveled), while the reflected light beam from a biological tissue consists of multiple echoes determined by the optical reflectivity of structures within the sample. These two reflected light beams (the reference and sample arms) are recombined at the partially reflecting mirror, creating an interference signal that is directed towards a photodetector for reading. The light source is coupled with He-Ne laser guidance beam for visualization (Fig. 1). Varying the position of the reference mirror in the optical delay line allows investigation of different tissue depths, because interference occurs when the reference delay arm distance is equal to the distance to a surface or internal reflecting structure within tissue in the sample arm. The pattern of interference created by the two recombined light beams is plotted on a logarithmic two-dimensional (2-D) scale to reconstruct an image of the structures with the biological sample, analogous to "B mode" echo image construction.[21] By obtaining successive parallel longitudinal OCT measurements, the images can be combined to create high-resolution three-dimensional (3-D) images of the complex biological specimens.

In addition to the structural images obtained by OCT technology, highly spatially localized flow and movement characteristics can be obtained from information contained in the Doppler shift of the reflected interference signal, referred to as optical Doppler tomography (ODT).[22] ODT allows non-invasive spatially localized imaging of tumor neovasculature and monitoring of changes in blood flow.[23] ODT works via the mechanism where incident coherent light at a central optical frequency enters the tissue and a small fraction of the reflected light is Doppler shifted by moving red blood cells, resulting in OCT interference fringe changes. In contrast, light scattered exclusively by static constituents has little or no frequency change.[6]

The Golden Syrian Hamster cheek pouch (HCP) 9,10-dimethyl-1,2-benzanthracene (DMBA) malignancy model is a standard animal model for investigating the development and diagnosis of oral cancer. This oral malignancy model is well established for upper airway tumor induction. HCP dysplasia and squamous cell carcinoma are comparable histologically to those of human oral cavity.[1,21] This study was conducted to demonstrate the feasibility of OCT and ODT for obtaining 3-D high-resolution optical images of oral malignancy and detecting changes that occur during malignant transformation using this animal model.

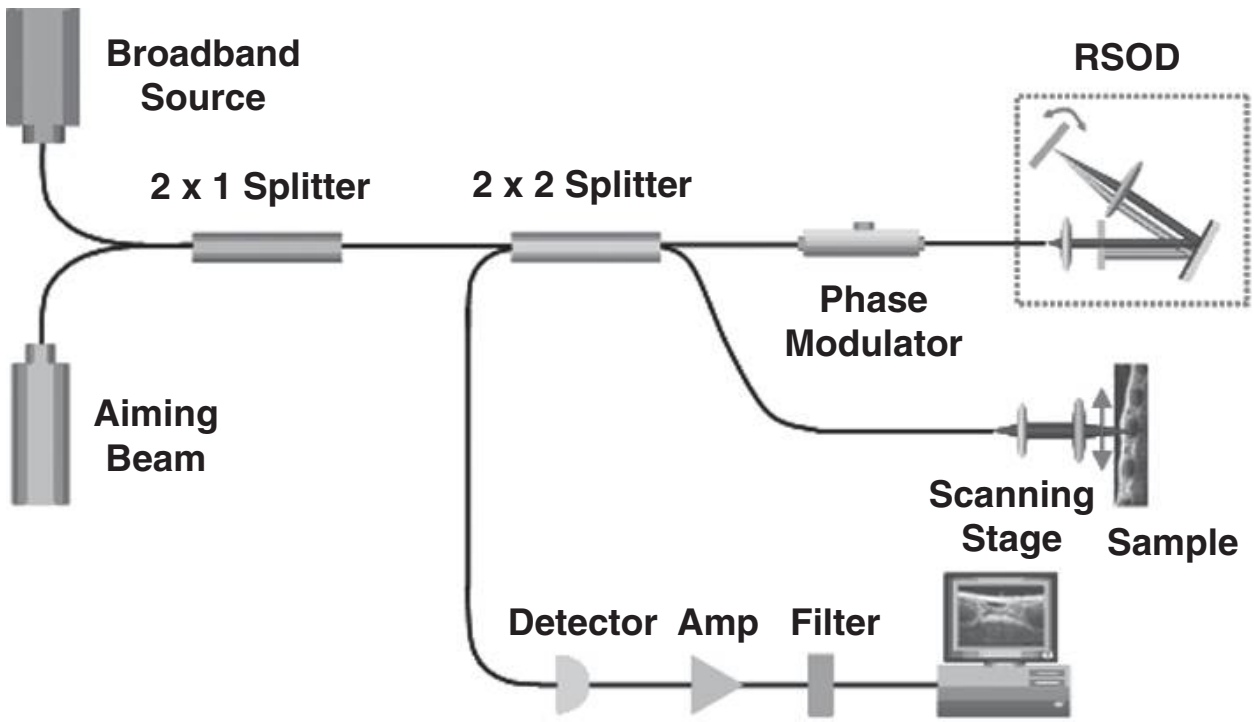

FIG. 1. Schematic of optical coherence tomography (OCT) imaging system. The light source of 1310-nm broadband super-luminescent diode with 70-nm bandwidth (full-width half-maximum [FWHM]) and the theoretical resolution of ~10–15 μm.

METHODS

Induction of carcinoma

The standard Golden Syrian Hamster (*Mesocricetus auratus*) cheek pouch model was used. In order to induce tumor growth, 0.5% DMBA (Sigma, St. Louis, MO 63178, USA) in mineral oil was applied three times per week to each of 30 female right HCP until carcinoma was observed. Mineral oil was applied to the left HCP to serve as a control for imaging and analysis. Previous studies have shown that DMBA has no effect on the contralateral cheek,[26,27] allowing the untreated cheek pouch to be used as a control. All HCP were examined for developing leukoplasia, erythroplasia, or tumor over a 4–16-week period. Mild to severe dysplasia developed in 3–6 weeks, with squamous cell carcinoma evident at 8–10 weeks.[28]

Animal treatment and imaging procedures

Animal treatment was compliant with ARC guidelines at University of California–Irvine (97-1972 and 2002-2397). Hamsters were anesthetized using inhalation anesthesia (isoflurane, 99.9% per mL; Abbott Laboratories, Chicago, IL) in a chamber. After prolonged application of DMBA and mineral oil, hamsters were examined for signs of oral cancer. If appropriate tumor growth or dysplasia was observed, hamsters were further anesthetized with intraperitoneal 2:1 ketamine HCl (100 mg/mL)/xylazine (20 mg/mL) at a dose of 0.75 cc/kg. In order to prevent hypothermia in the animals during anesthesia and imaging, the hamsters were placed in Mylar wrapping blankets and a thermal sock.

Optical coherence tomography and flexible fiberoptic probe prototype

For this study, a fiber-based OCT system that has 1300-nm center wavelength was employed. The OCT system used in this study—a superluminescent diode source—delivered an output power of 10 mW at a central wavelength of 1310 nm with a full-width half-maximum (FWHM) of 70 nm.

FWHM of the source determines the coherence length and governs axial resolution. Our source has 10-μm axial resolution. The spectral shape and FWHM of BBS1310 source is near Gaussian, close to optimal for OCT systems.

A visible aiming beam (633 nm) is used to find and locate the exact imaging position on the sample. In the reference arm, a rapid-scanning optical delay line was used that employs a grating to control the phase and group delays separately so that no phase modulation is generated when the group delay is scanned. The phase modulation is generated through an electrooptic phase modulator that produces a carrier frequency. The axial line scanning rate is 400 Hz, and the modulation frequency of the phase modulator is 500 kHz. Reflected beams from the two arms are recombined in the interferometer and detected on a photodetector. The interference signal is observed only when the optical path length difference between sample and reference arms is less than the coherence length of the source. The detected optical interference fringe intensity signals are bandpass filtered at the carrier frequency. Resultant signals are then digitized with an analog-digital converter (which performs 12-bit with 5 MHz) and transferred to a computer, where the structural image is generated.

Flexible fiber optic OCT probes were constructed from single-mode fiber patch cord (ThorLabs, Newton, NJ). The bare-ended fiber was attached to a 0.50-mm-diameter GRIN lens (NSG America, Irvine, CA), using optical adhesive (Optical Adhesive no. 68; Norland Products, Cranbury, NJ) under a microscope. A right-angle light path was achieved by a 0.5-mm prism.[24] The probe was placed in fluorinated ethylene propylene (FEP) tubing (17-gauge thin wall, Zeus, Orangeburg, SC) for added fiber support.

Imaging

Imaging was performed under anesthesia *in vivo* premortem, as well as *ex vivo* post-mortem. In order to image the tumors, the HCP were everted from the oral cavity and fixed in position with a specially designed stabilizing clamp (Fig. 2).

The cheek pouch and hamster were placed together on a 1-inch Travel Linear Translator (PT1; Thorlabs, Newton, NJ). OCT images were repeatedly obtained; after each image, the linear stage (linear translator) was moved 25 μm. This resulted in a stack of OCT images taken at 25-μm sampling intervals over the region of interest.

The cheek pouches were immediately excised after sacrifice and prepared for OCT/ODT imaging. The tissue section was stretched over cork and pinned using 0.20-mm insect pins. The cheek pouches were then covered with a thin layer of KY Gel to prevent the desiccation of the tissue during the imaging process (Johnson & Johnson Product Inc., Princeton, NJ). Triangular shaped notches were cut at opposite ends of the tissue to document a line of image acquisition. During both *in vivo* and *ex vivo* measurements, the cheek pouches were continuously irrigated with isotonic saline at room temperature to avoid dehydration of the tissue. A visible wavelength He-Ne laser guide beam was used to position the samples for OCT/ODT imaging. Pins were then used to mark the imaged area. After the animal was sacrificed, the tissue was harvested and prepared for standard paraffin section hematoxylin and eosin (H&E) staining and histological evaluation.

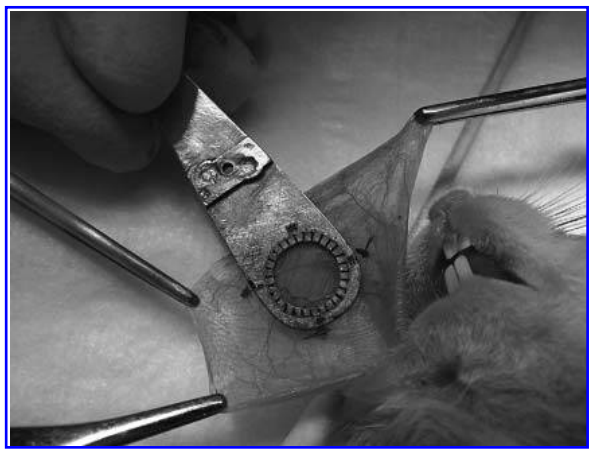

FIG. 2. Photograph of a hamster after preparation for *in vivo* optical coherence tomography (OCT) imaging.

Histology and matching

Previously described characteristics were examined to determine the degree of dysplasia/malignancy: healthy, hyperkeratosis, mild dysplasia, moderate dysplasia, severe dysplasia, carcinoma-in-situ, squamous cell carcinoma (SCC; Table 1.[26–28] The following characteristics were examined in OCT/ODT imaging: Drop-shaped rete ridges, irregular epithelial stratification, individual cell keratinization, basal cell hyperplasia, loss of intercellular adherence, loss of polarity, hyperchromatic nuclei, increased nucleo-cytoplasmic ratio, anisocytosis, pleomorphic cells and nuclei, abnormal mitotic figures, and increased mitotic activity. Epithelial invasion was characterized by the loss of visible basement membrane.

The presence of dysplasia and malignancy in the 3-D images were qualitatively assessed by the above characteristics. Each scorer evaluated all data in a single session, which took place once all data accrual was complete. A second reevaluation of all images, by the same scorers in a single session 3–4 months later, was used to evaluate intraobserver variability.

Histology slides were later imaged using an Olympus BH2 light microscope (with a 4 and 6.3 objective lens). An Olympus DP10 camera was used to photograph histology sections that corresponded to the OCT images of the section imaged.

Successive 2-D OCT and corresponding histology images were imported into a 3-D imaging program (3-D Doctor, Able Software, Lexington, MA) for graphic display, rotational imaging, cross sectional analyses, surface rendering, and stereo images. The 2-D OCT and histologic images for the particular section of tissue were then compiled into a 3-D assembled image.

RESULTS

Mild to severe dysplasia developed at 3–6 weeks, progressing to squamous cell carcinoma and/or tumor at 8–10 weeks. *In-vivo* three dimensional OCT imaging techniques were obtained automatically at weekly intervals in HCP during carcinogenesis development demonstrated excellent resolution. Progressive alteration in tissue structure, as well as delineation of tumor boundaries, where the shadowed and raised section of the image indicates the location of the tumor, was apparent in the cross-sectional single slice images of OCT with its corresponding histology (Fig. 3). In addition to the clear delineation of tumor boundaries in malignant tissues, Figure 4 shows 3-D images, with the corresponding 2-D image and histology of a normal cheek pouch. Clear delineation between the epithelium, mucosa, and submucosal layers of the tissue is still evident, including a blood vessel, which is only seen in Figure 4d due to angle differentiations between the OCT machine and the cheek pouch. Blood vessels are only evident in OCT images when the blood vessel runs at an approximately 90° angle to the area of the tissue being imaged, showing a cross-sectional image of the blood vessel as seen in Figure 4. Figure 5 shows the three stages of imaging—*in vivo*, *ex vivo* formalin imaging, and corresponding histology—elucidating how histological preparation of the tissue can alter the tissue by desiccation and some loss of structure. The continual tissue desiccation is illustrated by the decrease in contrast between the epithelium, and especially the mucosa, and submucosal layers within the 3-D histologic image, as opposed to a much more distinct contrast between these tissue layers in the 3-D OCT image, as well as the image taken after the tissue had been stored in formalin.

The 3-D OCT images could be viewed at rotating angles, "sectioned" at any level, or displayed stereoscopically using standard display algorithms, thereby enhancing delineation of structural changes and surface margins of the tumor. In addi-

TABLE 1. SPECIFICATIONS OF THE SLD-OCT SYSTEM

Type of OCT	*Fiber-based system*
Source type	Superluminescent diode
Center wavelength	1300 nm
FWHM of source	70 nm
Axial resolution	10 μm
Lateral resolution	10 μm
Measuring depth	2 mm
Imaged size	20 mm
SNR	80 dB
Image acquisition time	>1 frame per second for one image with 100 × 100 pixels

SLD, superluminescent diode; OCT, optical coherence tomography; FWHM, full-width maximum; SNR, signal-to-noise ratio.

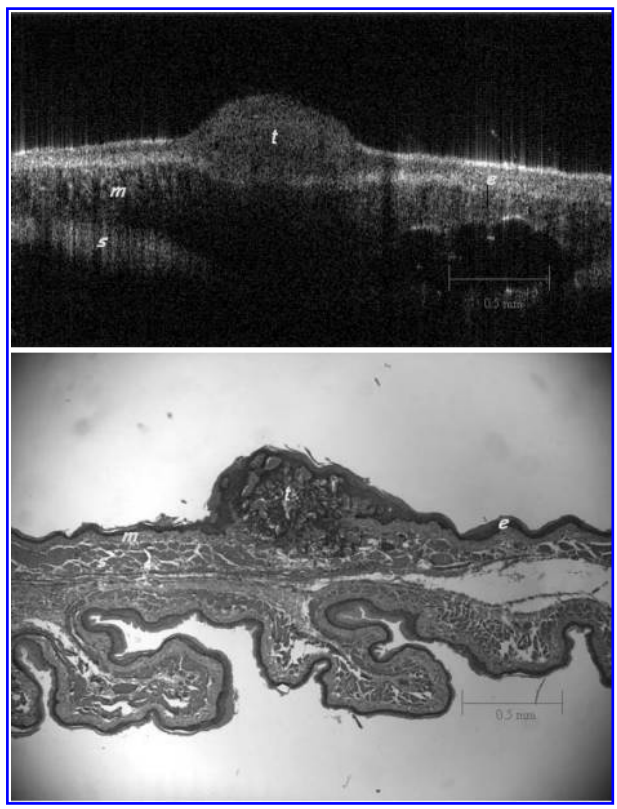

FIG. 3. Two-dimensional *in vivo* optical coherence tomography (OCT) image of a hamster cheek pouch (**A**) with corresponding histology (**B**). e, squamous epithelium; m, mucosa; s, submucosa; t, malignant tissue.

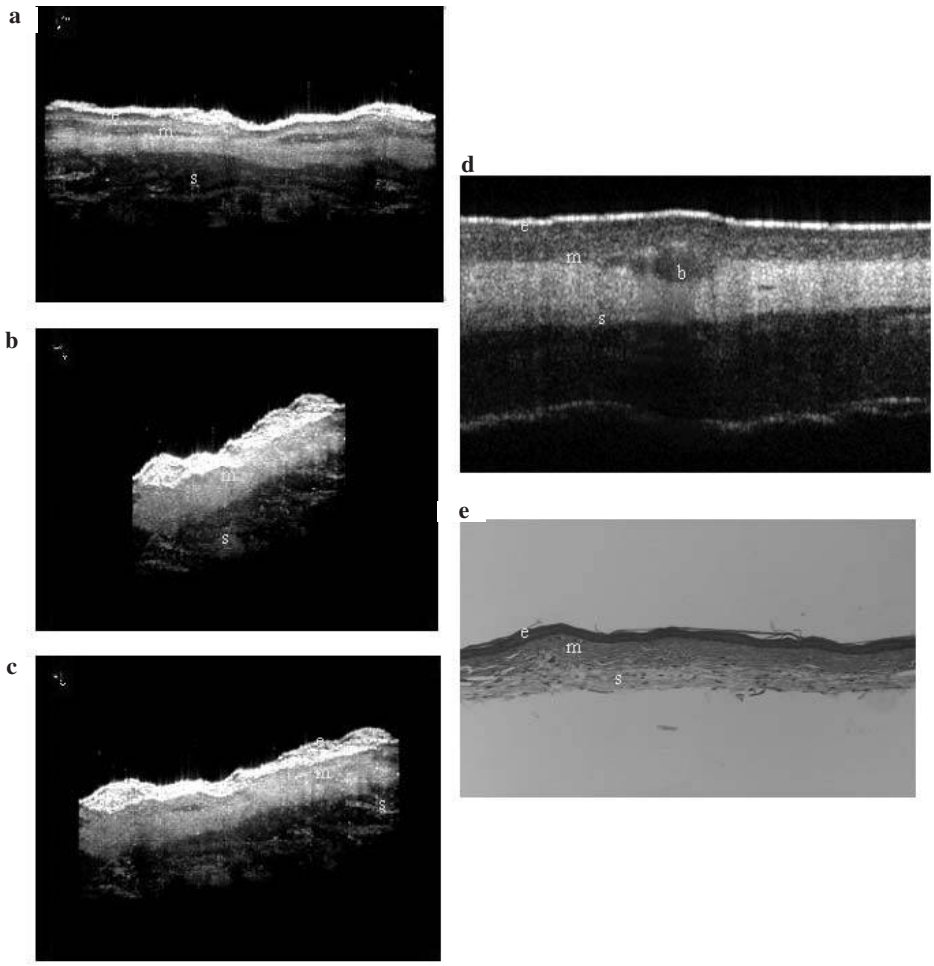

FIG. 4. Different views of a three-dimensional normal hamster cheek pouch (**a–c**) with its corresponding two-dimensional image, all taken *in vivo* (**d**), and histologic image (**e**). e, squamous epithelium; m, mucosa; s, submucosa; b, blood vessel.

tion, reconstruction of spatially resolved ODT imaging illustrated the presence of blood vessels through 3-D reconstruction of these blood vessel structures imaged *in vivo* at resolutions of 15–30 μm (Fig. 6).

With the progression through dysplasia to malignancy, tissue organization became increasingly disrupted to the point of almost complete disappearance as demonstrated by the 3-D OCT images.

DISCUSSION

OCT technology for medical applications is rapidly advancing. OCT has many advantageous characteristics for medical diagnostics including potential for very high resolution, "noninvasive" optical imaging of surface and subsurface complex tissue structure and function. Currently, this technology allows for minimally invasive *in vivo* imaging of complex tissues to a depth of 1–3 mm, with very high resolution of 10–15 μm with the potential for much higher resolutions of 1–2 μm.[10,12,22,29] With further optimization of light sources, acquisition methods, processing algorithms, and endoscopic probes, the capabilities of OCT for medical applications will continue to expand.

Oral cancer detection is a potentially ideal application for OCT technology, due to the easy accessibility of the oral cavity, a pattern of progression of oral cancer from dysplasia to malignancy, and because of difficulties in screening for oral cancer with existing invasive biopsy methods. In addition, the shallow depth of penetration of OCT is generally adequate for oral cancer detection, since most oral cancers originate near the mucosal surface. OCT can be performed repeatedly without significant risk in the oral cavity. In addition to structural OCT imaging, the ability to examine localized blood flow properties with ODT may provide additional insight into oral tissue abnormalities, especially when used in conjunction with one another. Future studies should help define the role of functional OCT in oral cancer evaluation.

A major step in the evolution of OCT diagnostics will involve development of 3-D OCT and functional OCT imaging methodologies. 3-D imaging will be important for accurate delineation of tumor or dysplasia margins, elucidation of regional changes in patterns and progression of lesions, and in imaging research. 2-D and 3-D ODT evaluation of micro-vasculature, neovascu-

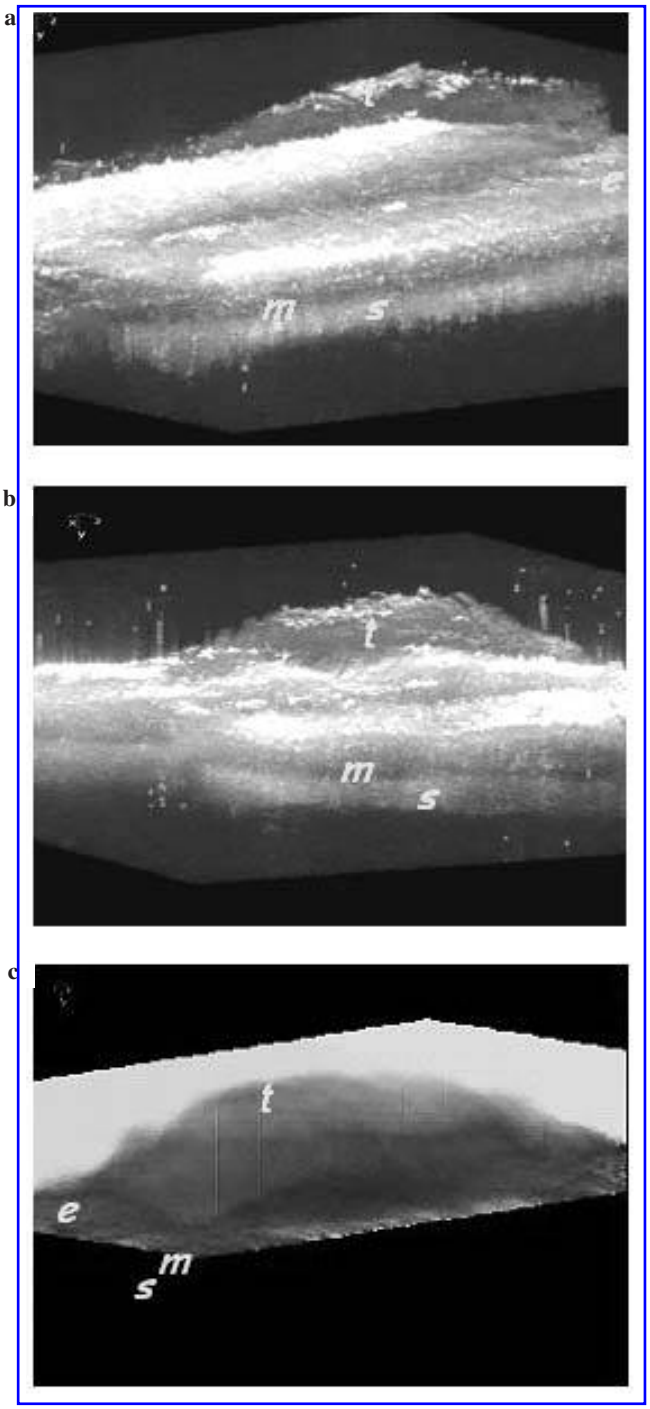

FIG. 5. Different views of three-dimensional optical coherence tomography (OCT) images of a malignant hamster cheek pouch *in vivo* (**a**), in formalin (**b**), and with their corresponding histology (**c**). The *in vivo* image appears larger than the image of the 3-D image of the same tissue after treatment with formalin. The 3-D OCT formalin image corresponds more closely to the histology, thus pointing out the changes in the tissue—the decrease in distinction between the epithelium, mucosa, and submucosa—that take place due to histological preparation of the specimen.[23] e, squamous epithelium; m, mucosa; s, submucosa; t, malignant tissue.

larization, blood flow properties (including micro-capillary blood velocity and volume) may be of particular value in assessing angiogenesis during carcinogenesis. Similarly, evaluation of response to therapy will require 3-D OCT and functional OCT imaging. 3-D OCT and ODT, when used simultaneously, may be useful to help determine more specific surface boundaries of the malignancy for more efficient biopsy (OCT), as well as determination of the amount of blood flow to the area (ODT), potentially helping indicate the stage of the malignancy.

These findings illustrate the feasibility of 3-D imaging of oral dysplasia and malignancy using OCT/ODT. Future studies using higher resolution systems and clinical validation in patients with airway dysplasia and malignancy will be needed to determine the clinical role of OCT in oral cancer detection.

CONCLUSION

This study has demonstrated the feasibility of 3-D OCT and ODT for *in vivo* imaging of oral cavity carcinogenesis development. This study has shown the capability of OCT to obtain high-resolution images in the oral cavity associated with dys-

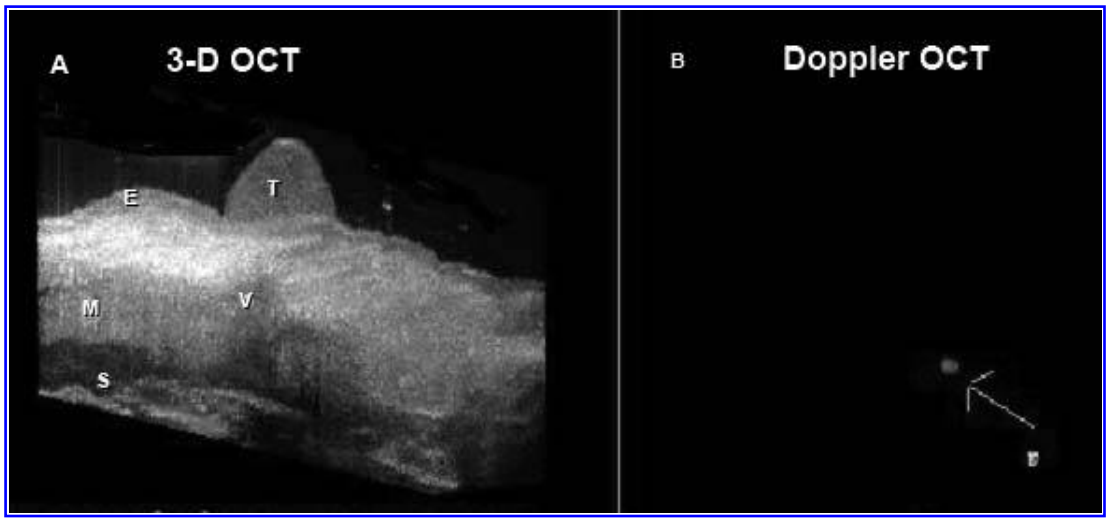

FIG. 6. Three-dimensional *in vivo* optical coherence tomography (OCT) image of hamster cheek pouch tumor (**A**) with the corresponding *in vivo* ODT image with a neovascular growth around the tumor (**B**). E, squamous epithelium; M, mucosa; S, submucosa; T, malignant tissue; V, vasculature.

plasia and oral cancer in the HCP model. Successful development of endoscopic 3-D OCT for the oral cavity and other sites requires optimization of rigid and flexible fiber-optic 3-D OCT probes, 3-D analysis algorithms, and methods for 3-D display in real-time. With improved resolution to the micron level, differentiation between benign and malignant lesions may become possible non-invasively. OCT should be of considerable value in assessing effects of drugs and medications, angiogenesis inhibitors, radiation, and chemotherapy in the treatment of oral cancer. Advances in 3-D OCT imaging could be applicable to other areas of endoscopic imaging for a range of medical conditions and tissue sites, including gastrointestinal, pulmonary, cardiac, and urinary systems. Once optimized, OCT may provide the capability of obtaining non-invasive high-resolution real-time optical images of superficial tissues using flexible fiberoptic probes for a range of medical applications.[11]

ACKNOWLEDGMENTS

This study was supported in part by Philip Morris (research grant PM-USA-32598), TRDRP (grant 9RT-0094), Air Force (grant F49620-00-10371), and NIH (grants EB-00293, NCI-91717, RR-01192, BES-86924).

REFERENCES

1. Ebihara, A., Krasieva, T.B., Liaw, L.H., et al. (2003). Detection and diagnosis of oral cancer by light-induced fluorescence. Lasers Surg. Med. 32, 17–24.
2. Motamedi, M., Johnigan, R., Bell, B., et al. (2000). Fluorescence guided optical coherence tomography for early detection of epithelial neoplasia. Presented at the Lasers and Electro-Optics Society 2000 Annual Meeting (LEOS), Rio Grande, Puerto Rico.
3. Pitris, C., Drexler, W., Ghanta, R.K., et al. (2000). *In vivo* and *ex vivo* high-resolution evaluation of neoplastic tissues with optical coherence tomography. Presented at the Conference on Lasers and Electro-Optics (CLEO) 2000, San Francisco.
4. McNichols, R.J., Gowda, A., Bell, B.A., et al. (2001). Development of an endoscopic fluorescence image guided OCT probe for oral cancer detection. SPIE Proc. 4254, 23–30.
5. Otis, L.L., Everett, M.J., Sathyam, U.S., et al. (2000). Optical coherence tomography: a new imaging technology for dentistry. J. Am. Dent. Assoc. 131, 511–514.
6. Bouma, B.E., Tearney, G.J. (2002). *Handbook of Optical Coherence.* New York: Marcel Dekker.
7. Bouma, B.E., and Tearney, G.J. (1999). Power-efficient nonreciprocal interferometer and linear-scanning fiber-optic catheter for optical coherence tomography. Optics Lett. 24, 531–533.
8. Tearney, G.J., Brezinski, M.E., Southern, J.F., et al. (1997). Optical biopsy in human gastrointestinal tissue using optical coherence tomography. Am. J. Gastroenterol. 92, 1800–1804.
9. Bouma, B.E., and Tearney, G.J. (2002). Clinical imaging with optical coherence tomography. Acad. Radiol. 9, 942–953.
10. Tearney, G.J., Brezinski, M.E., Bouma, B.E., et al. (1997). *In vivo* endoscopic optical biopsy with optical coherence tomography. Science 276, 2037–2039.
11. Izatt, J.A., Kulkami, M.D., Kobayashi, K., et al. (1997). Optical coherence tomography for biodiagnostics. Optics Photonics News 8, 42–47.
12. Tadrous, P.J. (2000). Methods for imaging the structure and function of living tissues and cells. 1. Optical coherence tomography. J. Pathol. 191, 115–119.
13. Fujimoto, J.G., Pitris, C., Boppart, S.A., et al. (2000). Optical coherence tomography: an emerging technology for biomedical imaging and optical biopsy. Neoplasia 2, 9–25.
14. Fujimoto, J.G. (2001). Optical coherence tomography. Comp. Rend. Acad. Sci. Ser. IV Phys. Astrophys. 2, 1099–1111.
15. Swanson, E.A. (1999). Optical coherence tomography: principles, instrumentations, and applications. Presented at the Conference on Lasers and Electro-Optics (CLEO) '99, Baltimore.
16. Pan, Y., Lankenou, E., Welzel, J., et al. (1996). Optical coherence-gated imaging of biological tissues. IEEE. Quantum Electr. 2, 1029–1034.
17. Fujimoto, J.G., Bouma, B., Tearney, G.J., et al. (1998). New technology for high-speed and high-resolution optical coherence tomography. Ann. NY Acad. Sci. 838, 95–107.
18. Fujimoto, J.G., Boppart, S.A., Tearney, G.J., et al. (1999). High-resolution in vivo intra-arterial imaging with optical coherence tomography. Heart 82, 128–133.

19. Fujimoto, J.G., Boppart, S.A., Pitris, C., et al. (1999). Optical coherence tomography: a new technology for biomedical imaging. Jpn. J. Laser Med. Surg. 20, 141–168.
20. Fujimoto, J.G., Drexler, W., Morgner, U., et al. (2000). Optical coherence tomography: high-resolution imaging using echoes of light. Optics Photonics News 11, 24–31.
21. Charoenbanpachon, S., Krasieva, T., Ebihara, A., et al. (2003). Acceleration of ALA-induced PpIX fluorescence development in the oral mucosa. Lasers Surg. Med. 32, 185–188.
22. Zhihua, D., Hongwu, R., Yonghua, Z., et al. (2002). High-resolution optical coherence tomography over a large depth range with an axicon lens. Optics Lett. 27, 243–245.
23. Herz, P.R., Chen, Y., Aguirre, A., et al. (2004). Ultrahigh resolution optical biopsy with endoscopic optical coherence tomography. Optics Express 12, 3532–3542.
24. Huang, D., Swanson, E.A., Lin, C.P., et al. (1991). Optical coherence tomography. Science 254, 1178–1181.
25. MacDonald, D.G. (1981). Comparison of epithelial dysplasia in hamster cheek pouch carcinogenesis and human oral mucosa. J. Oral Pathol. 10, 186–191.
26. Wilder-Smith, P., Osann, K., Hanna, N., et al. (2004). *In vivo* multiphoton fluorescence imaging: a novel approach to oral malignancy. Lasers Surg. Med. 35, 96–103.
27. Wilder-Smith, P., Krasieva, T., Jung, W.G., et al. (2005). Noninvasive imaging of oral premalignancy and malignancy. J. Biomed. Optics 10, 51601.
28. Wilder-Smith, P., Jung, W.G., Brenner, M., et al. (2004). *In vivo* optical coherence tomography for the diagnosis of oral malignancy. Lasers Surg. Med. 35, 269–275.

Address reprint requests to:
Dr. Matt Brenner
Pulmonary and Critical Care Division
UC Irvine Medical Center
Bldg. 53, Rm. 119
101 City Drive South
Orange, CA 92868

E-mail: mbrenner@uci.edu

This article has been cited by:

1. Giriraj K. Sharma, Marc Rubinstein, Christian Betz, Brian J.-F. WongOptical Coherence Tomography of Malignancies of the Head and Neck 589-599. [CrossRef]
2. Veronika Volgger, Herbert Stepp, Stephan Ihrler, Marcel Kraft, Andreas Leunig, Parag M. Patel, Malavika Susarla, Kathleen Jackson, Christian S. Betz. 2013. Evaluation of optical coherence tomography to discriminate lesions of the upper aerodigestive tract. *Head & Neck* **35**:11, 1558-1566. [CrossRef]
3. Marc Rubinstein, Davin Chark, Brian WongOptical Coherence Tomography of the Human Oral Cavity and Oropharynx . [CrossRef]
4. Bahar Davoudi, Andras Lindenmaier, Beau A. Standish, Ghassan Allo, Kostadinka Bizheva, Alex Vitkin. 2012. Noninvasive in vivo structural and vascular imaging of human oral tissues with spectral domain optical coherence tomography. *Biomedical Optics Express* **3**:5, 826. [CrossRef]
5. Randy Hou, Tho Le, Septimiu D Murgu, Zhongping Chen, Matt Brenner. 2011. Recent advances in optical coherence tomography for the diagnoses of lung disorders. *Expert Review of Respiratory Medicine* **5**:5, 711-724. [CrossRef]
6. Shengwen Calvin Li, Lisa May Ling Tachiki, Jane Luo, Brent A. Dethlefs, Zhongping Chen, William G. Loudon. 2010. A Biological Global Positioning System: Considerations for Tracking Stem Cell Behaviors in the Whole Body. *Stem Cell Reviews and Reports* **6**:2, 317-333. [CrossRef]
7. B.J. Vakoc, G.J. Tearney, B.E. Bouma. 2009. Statistical Properties of Phase-Decorrelation in Phase-Resolved Doppler Optical Coherence Tomography. *IEEE Transactions on Medical Imaging* **28**:6, 814-821. [CrossRef]
8. Kelly A. Kreuter, Sari B. Mahon, David S. Mukai, Jianping Su, Woong-Gyu Jung, Navneet Narula, Shuguang Guo, Nicole Wakida, Chris Raub, Michael W. Berns, Steven C. George, Zhongping Chen, Matthew Brenner. 2009. Detection and monitoring of early airway injury effects of half-mustard (2-chloroethylethylsulfide) exposure using high-resolution optical coherence tomography. *Journal of Biomedical Optics* **14**:4, 044037. [CrossRef]
9. Cheng-Kuang Lee, Meng-Tsan Tsai, Hsiang-Chieh Lee, Hsin-Ming Chen, Chun-Pin Chiang, Yih-Ming Wang, C. C. Yang. 2009. Diagnosis of oral submucous fibrosis with optical coherence tomography. *Journal of Biomedical Optics* **14**:5, 054008. [CrossRef]
10. Meng-Tsan Tsai, Cheng-Kuang Lee, Hsiang-Chieh Lee, Hsin-Ming Chen, Chun-Pin Chiang, Yih-Ming Wang, Chih-Chung Yang. 2009. Differentiating oral lesions in different carcinogenesis stages with optical coherence tomography. *Journal of Biomedical Optics* **14**:4, 044028. [CrossRef]
11. C. C. Yang, Meng-Tsan Tsai, Hsiang-Chieh Lee, Cheng-Kuang Lee, Chuan-Hang Yu, Hsin-Ming Chen, Chun-Pin Chiang, Cheng-Chang Chang, Yih-Ming Wang, C. C. Yang. 2008. Effective indicators for diagnosis of oral cancer using optical coherence tomography. *Optics Express* **16**:20, 15847. [CrossRef]
12. S. Fedele, L. Lo Russo, C. Mignogna, S. Staibano, S.R. Porter, M.D. Mignogna. 2008. Macroscopic classification of superficial neoplastic lesions of the oral mucosa: A preliminary study. *European Journal of Surgical Oncology (EJSO)* **34**:1, 100-106. [CrossRef]
13. Meng-Tsan Tsai, Hsiang-Chieh Lee, Chih-Wei Lu, Yih-Ming Wang, Cheng-Kuang Lee, C. C. Yang, Chun-Ping Chiang. 2008. Delineation of an oral cancer lesion with swept-source optical coherence tomography. *Journal of Biomedical Optics* **13**:4, 044012. [CrossRef]
14. Desmond C. Adler, Yu Chen, Robert Huber, Joseph Schmitt, James Connolly, James G. Fujimoto. 2007. Three-dimensional endomicroscopy using optical coherence tomography. *Nature Photonics* **1**:12, 709-716. [CrossRef]
15. Matthew Brenner, Kelly Kreuter, David Mukai, Tanya Burney, Shuguang Guo, Jianping Su, Sari Mahon, Andrew Tran, Lillian Tseng, Johnny Ju, Zhongping Chen. 2007. Detection of acute smoke-induced airway injury in a New Zealand white rabbit model using optical coherence tomography. *Journal of Biomedical Optics* **12**:5, 051701. [CrossRef]